www.ijbem.org

Regional impedance pneumography heterogeneity during airway opening pressure chirp oscillations

Javier Gracia^a, Ville-Pekka Seppä^a, Jari Viik^a

^aDepartment of Electronics and Communications Engineering, Tampere University of Technology, BioMediTech, Tampere, Finland

Correspondence: J Gracia, Tampere University of Technology, P.O. Box 692, FIN-33101 Tampere, Finland. E-mail: gracia.javier@tut.fi

Abstract. We hypothesise that a simultaneous use of impedance pnemography (IP) and force oscillation technique (FOT) has the potential to increase the accuracy of the second one in the assessment of the small airways. We conducted a preliminary study to understand the effects of FOT pressure oscillation in the IP signal.

Pressure chirps 1.35 seconds long providing a flat power spectrum from 0 to 35 Hz were imposed over tidal breathing for four sitting healthy subjects. Thoracic electrical resistivity changes where recorded simultaneously at three different axial levels of the thorax by an IP measurement system. Lung volume changes were extracted from the IP signals by subtracting the cardiac component by means of ensemble averaging. Chirp responses in airway opening flow and IP volume signals were separated from breathing using a time-varying bandpass filter. Consequently, complex ratio between airway opening flow chirps (\dot{Q}_{ao}) and time derivative of IP chirps (\dot{Q}_{IP}) were compute for the three thorax levels $(H_{if} = \dot{Q}_{ao}/\dot{Q}_{IPm};_{\{m=1,2,3\}})$.

Results presented an antiresonat frequency response that could not be explained with the initial assumption that oscillations in the IP signal are solely related to alveolar volume changes. We concluded that there is an additional phenomenon reflecting FOT oscillations into the IP signal. We discuses two possibilities: alveolar pressure oscillations modulate the pulmonary capillaries blood volume thus altering tissue resistivity density; or vibrations in the skin-electrode cause an oscillating motion artefact.

Keywords: Impeance Pnemography; Forced Oscillation Technique; Impulse oscillometry; Small Airways; Lung mechanics;

1. Introduction

Forced oscillation technique (FOT) is a noninvasive respiratory test with more than 50 years of history. In FOT small magnitude pressure oscillations are imposed over tidal breathing at the airway opening. The complex ratio of the resulting airflow (\dot{Q}_{ao}) to the delivered pressure (P_{ao}) is defined as the input impedance ($Z_{in}=P_{ao}/\dot{Q}_{ao}$); a measurement of the respiratory system mechanical properties [Peslin et al., 2011]. In recent years FOT has won popularity as it proved to detect small airway dysfunctions that are unnoticed by traditional spirometry. However, because input impedance reflects mechanical properties of the whole respiratory system, diseases of the parenchyma, pleura, and chest wall may produce abnormal data that is undisguisable from small airways diseases [Berger et al. 2015]. This is one of the main reasons holding FOT to be accepted into general clinical practice.

Impedance pneumography (IP) is a noninvasive lung function measurement technique. IP uses four surface skin electrodes to record changes in the thoracic electrical resistivity. The thoracic resistivity signal has a cardiac and a respiratory component. The cardiac component is caused by the blood redistribution within the thorax during each heartbeat. In IP, it is consider an interference and is removed from the signal. The respiratory component emerges from structural changes in the lung tissue during respiration. Specifically, the thinning of the alveolar walls with increasing air leads to a proportional increment in tissue resistivity density [Nopp et al. 1997].

It has been observed that when FOT and IP are used simultaneously, airway opening pressure oscillations reflect in the IP signals recorded at the thorax [Gracia et al. 2011] [Gracia et al. 2015]. We hypotheses that, since the IP signal is linked to alveolar wall changes, resulting oscillations may

be related to the mechanical properties of the alveoli, as well as the small airways preceding the alveolar sacs. Therefore, a combined FOT-IP method has the potential to assess small airways diseases independently of other respiratory system conditions.

This article presents a novel FOT approach optimized for the combined use with IP. This lies on chirp oscillations pressure signals, and time variant band pass filter. The combined method was validated against traditional sinusoidal pressure oscillation. Consequently, it was used to calculate the complex ratio between airway opening flow and IP oscillations $(H_{ij} = \dot{Q}_{ao}/\dot{Q}_{IPm})$ at 3 levels of the thorax for 4 different healthy subjects. The article describes the set-up, data analysis, and discuses two possible explanation for the results based on literature.

2. Material and Methods

2.1. Apparatus

Figure 1 shows a block diagram of the overall system. A personal computer (PC) provided, by a means of a digital to analog converter (DAC) (NI6251, National Instruments), an electrical signal whose characteristics are described later. Using a self-made power amplifier (Amp.) (based on a TDA7266, STMicroelectronics), this signal drove a 250 mm diameter acoustic suspension loudspeaker mounted in a 50 mm high conical frustum ending in an opening of 30 mm diameter. The pressure signal generated by the loudspeaker was transmitted to the subject thought a Fleisch pneumotachograph and a mouth piece.

A perpendicular open rigid tube of 8mm i.d. and 15cm long between pneumotachograph and mouth piece worked as a mechanical low pass filter. Tube offered low resistance to low tidal breathing rates and linearly increasing resistances for the pressure oscillations -theoretical resistance with frequency $X_l(f) = 2\pi \cdot f \cdot 896 \left[kg \cdot s^{-1} \cdot m^{-4} \right]$ [Bauer BB. 1954]-.

The pneumotachograph was connected to a differential pressure transducer (HCLA02X5EB, SensorTechnics) measuring airflow (\dot{Q}_{ao}). Pressure at the airway opening (P_{ao}) was measured by a pressure transducer (DCXL10DS, Honeywell). Transducers were connected to the multipurpose conditioning device MP35 (BioPac Systems) which included an electrocardiogram amplifier. All three signals were digitalized at 1 kHz and sent to the PC.

Flow and pressure sensor were calibrated by a 3-litre piston. Frequency characteristics of the whole system were assessed from 0 to 35 Hz. We used the method suggested by Brusasco et al. [Brusasco et al. 1994], based in a reference impedance made of a bundle of pipelets whose impedance was predicted theoretically.

IP signals were recorded using the HF2IS (Zurich Instruments) impedance spectroscope with the HF2TA (Zurich Instruments) current amplifier in a tetrapolar configuration. System was configured with a 1V 100kHz output signal and a 150Hz bandwidth filter.

A digital signal (*Sync*) was produce by the NI6251 DAQ and connected simultaneously to the MP35 and HF2IS devices to ensure synchronized signals.

2.2. Excitation signals

Two different kinds of pressure signals were used: single frequency sinusoids and broad band chirps. The amplitude of the pressure sine waves were controlled to be 6 cmH2O peak to peak for all frequencies independently of the load imposed. This was achieved by a feedback control system by means of a proportional integral control law acting in every sine cycle. Chirps were design to sweep from 0 to 35Hz in a period of 1.35 seconds. Nonlinear frequency response of the speaker was calibrated by adjusting the chirp's envelope for the pipelets reference impedance. It was set to amplitude of 6 cmH2O peak to peak for the whole working frequency range.

2.3. Experimental set up

As show in Figure 1, 4 pairs of electrodes where placed on the subjects allowing 3 IP measurement configurations (Table 1). The first pair of electrodes was placed on the arms between biceps and triceps brachia muscles. The second pair of electrodes was placed on the sides of the thorax on the midaxillary line at the height of the 5th intercostal line. The two other pairs were placed lower with a separation of 5 cm. An additional pair was placed in the upper chest and abdomen to record the ECG signal.

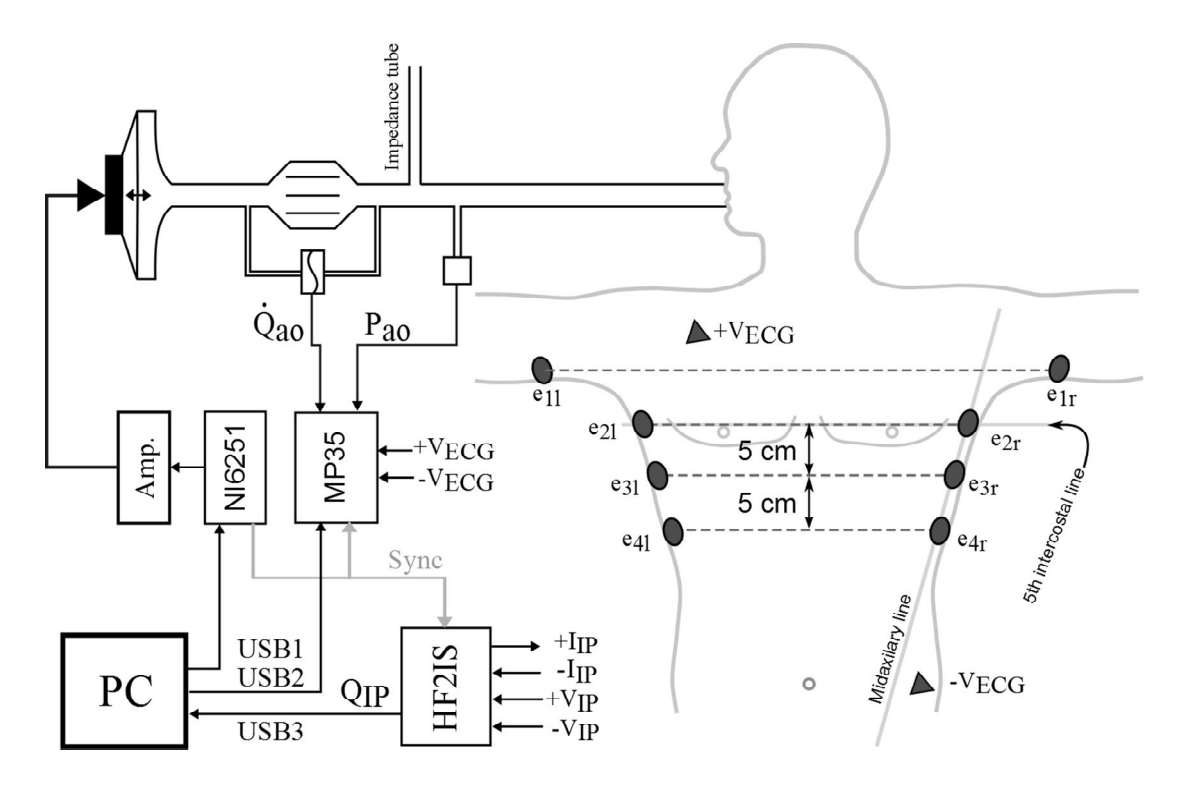


Figure 1. Overall system block diagram and electrodes location. Filled triangles and circles over the subject's silhouette represent ECG and IP electrodes respectively. IP electrodes were connected to the inputs of the HF2IS (+ I_{IP} , - I_{IP} , + V_{IP} , - V_{IP}) in three different configuration Table 1. Recorded signals were: airway opening pressure (P_{ao}), airway opening flow (\dot{Q}_{ao}), thorax electrical resistivity changes (Q_{IPm}), and electrocardiogram signal (V_{ECG}).

Test subjects sat in a comfortable position with the mouth at the height of the FOT device opening. The subjects were requested to hold their cheeks with their hands and perform tidal breathing thought the mouth piece during three different experiments: 60 seconds with no pressure oscillations for calibration purposes; 22 intervals of 25 seconds with integer frequencies sinusoidal oscillations between 2 Hz and 24 Hz; and 30 seconds with pressure chirps repeated periodically every 1.65 seconds.

Flow, pressure, ECG, and IP signals were recorded. Experiments were repeated for each electrode configuration (*m*) (Table 1) and for each subject. Test subjects consisted of two female and two male nonsmokers in ages between 26 and 32 years. IP electrodes were fastened with elastic bands and connection cables secured to the body with tape.

Table 1. Electrode connections to tetrapolar IP leads for each electrode configuration. Last four columns denote the label of the electrode (e_{xx}) connected to each of the four leads of the IP measurement system ($+I_{IP}$;- I_{IP} ;+ V_{IP} ;- V_{IP}) for each of the three electrode configuration (m) specified in the first column. Second column labels the recorded signals as used along the article.

Electrode configuration m	Measured Signal	Electrode to lead connection			
		$+I_{IP}$	$-I_{IP}$	$+V_{IP}$	$+V_{IP}$
1	Q_{IPI}	elr	e1l	e2r	e2l
2	Q_{IP2}	e2r	e2l	e3r	e3l
3	Q_{IP3}	e3r	e31	e4r	e4l

2.4. Data analysis

Before analysis, the cardiac component was removed from all IP signals using the enhanced ensemble average method described by Seppä et al. [Seppä et al. 2011]. Each IP signal was split in sections of cardiac cycle duration, defined by the R-peaks of the ECG signal. Sections were resized to the same time duration and averaged into a cardiogenic oscillation (CGO) template. The CGO template was again resized to the duration of each R-peak interval and subtracted from the original IP signal.

Result of the CGO filter for a representative IP signal recorded during chirp pressure oscillations is showed in Figure 2, labeled Q_{IPI-B} .

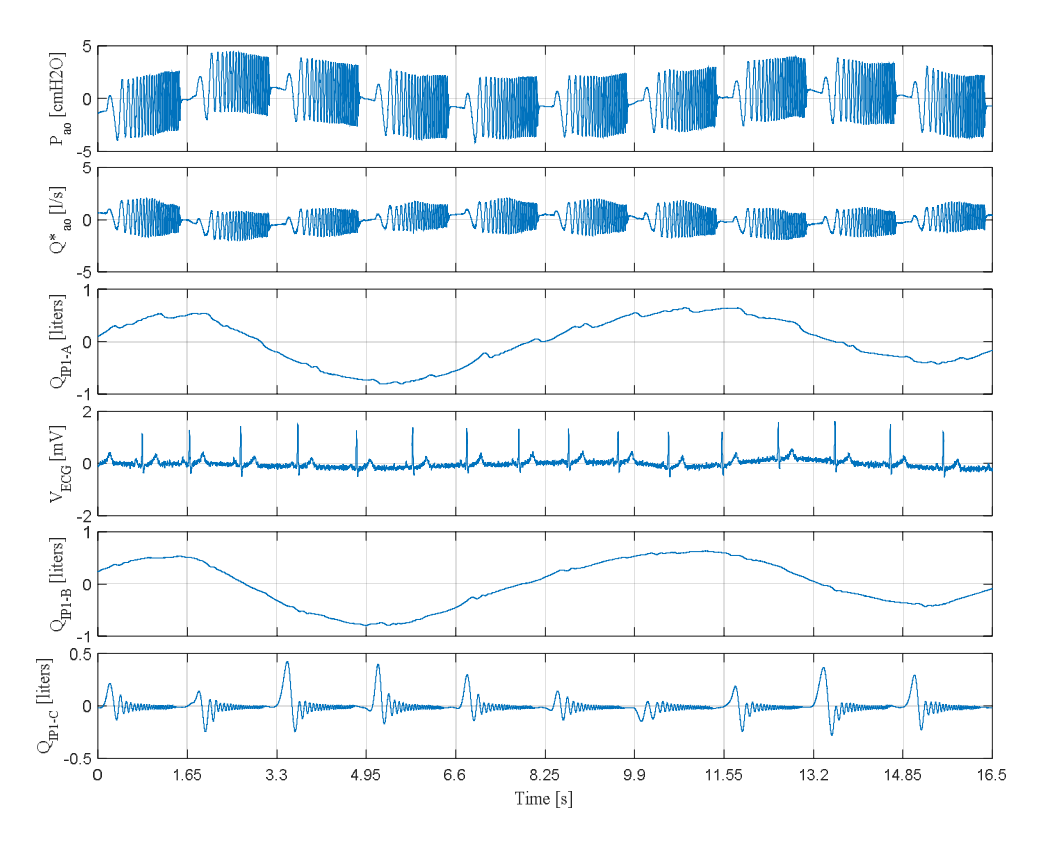


Figure 2. Representative recording and IP signal filtering results obtained during 10 chirp pressure oscillations. From top to button: airway opening pressure (P_{ao}) ; airway flow (\dot{Q}_{ao}) ; upper thorax resistivity changes for subject-1 (Q_{IPI_SI-A}) ; electrocardiogram signal (V_{ECG}) ; Q_{IPI_SI-A} signal after CGO removal (Q_{IPI_SI-B}) ; and Q_{IPI_SI-B} signal after the time-varying bandpass filter (Q_{IPI_SI-C}) . Notice that Q_{IPI_SI-C} represents volume changes, where amplitude decreases with frequency at a rate of $1/2\pi f$ respect to the equivalent flow signal. Time marks delimit the 1.65 seconds duration windows.

Tidal breathing

IP signals were calibrated to match the full lung volume changes for each patient and each electrode configuration. Calibration factor was calculated as the ratio of the standard deviations of the IP signal (Q_{IPm}) and the time integral of the flow signal (Q_{ao}) , both obtained during the 60 seconds tidal breathing recordings.

Single frequency sinusoids

For each group of 25 seconds recordings, the first 5 seconds were rejected. Airway opening pressure, airway opening flow, and IP signals were split into 7 seconds long windows with 50% overlap, and multiply by a hamming window of the same duration. The input impedance Z_{in} and coherence γ^2_{in} function between flow and pressure was compute for each window as explained in Appendix A. The flow ratio H_{ij} and coherence function γ^2_{ij} between flow and the time derivative of the IP signal (\dot{Q}_{IPm}) was compute for each window as explained in Appendix B.

Computed values were averaged for each oscillation frequency, subject, and electrodes configuration. Windows with coherence function below 0.95 were rejected.

Chirp signal

For the chirp oscillations recordings, airway opening pressure, airway opening flow, and IP signals were split into 1.65 seconds windows. Windows started 0.15 seconds before each pressure excitation chirp (Figure 2).

For all windows a time-varying bandpass filter was applied. This filter attenuated these frequencies not belonging to the chirp signal along the time window. The filter converted each time window to the time-frequency domain using the Gabor transform. Output was multiplied by the 2 dimensional function described by equation (1). Result was converted back to time domain using the inverse Gabor transform. A visual example of the process for an IP chirp window is showed in Figure 3. Result of the Gabor multiplier for a representative IP signal recorded during chirp pressure oscillations is showed in Figure 2, labeled Q_{IPI-C} .

$$f(t,f) = \exp \left\{ \sum_{k=0}^{\infty} \frac{e^{k}}{k} \frac{t^{2}}{2s_{f}^{2}} + \frac{f^{2}}{2s_{f}^{2}} \right\} \frac{\ddot{o}\ddot{o}}{2s_{g}^{2}}$$

$$f = \left(t - 0.15s\right) \frac{35Hz}{1.37s}; \tag{1}$$

$$t < 1.5s;$$

Input impedance Z_{in} and coherence function γ^2_{in} were computed for each pair of flow and pressure window as explained in Appendix A. Flow ratio H_{if} and coherence function γ^2_{if} were compute for each pair of flow and IP windows as explained in Appendix B. Computed values were averaged for each subject and electrodes configuration rejecting these windows with coherence function below 0.95.

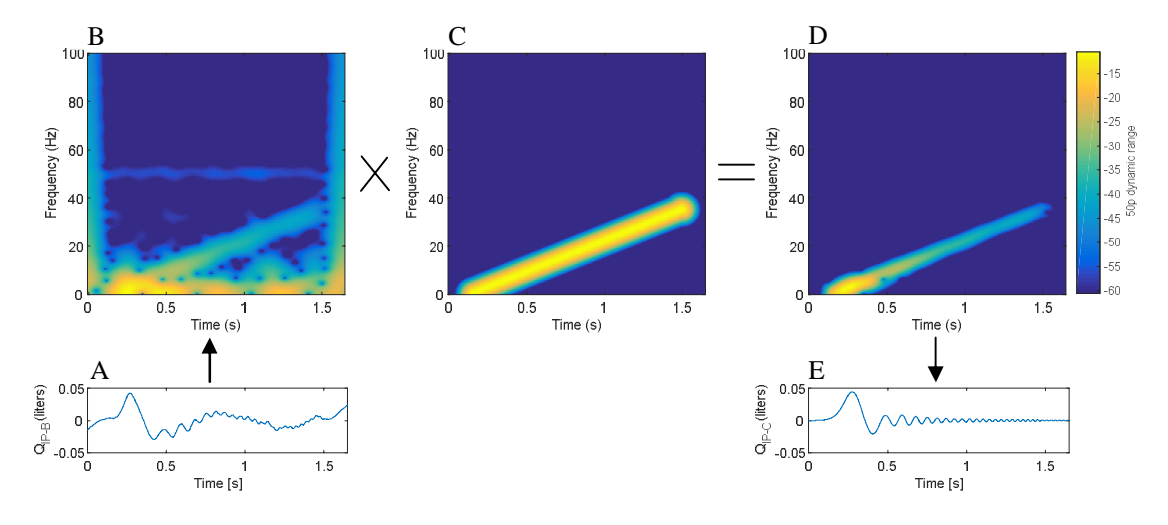


Figure 3. Time-varying filter applied to a representative IP window extracted from the Q_{IPI_SI-B} signal. A chirp oscillation mixed with respiration (A) is converted to the time-frequency domain (B) where it is multiplied by the Gabor multiplier (C) to extract the chirp component. Result (D) is converted back to time domain (E).

3. Results

Input impedances calculated from sinusoidal and chirp oscillations were compared for each subject (Figure 4). Sinusoids' input impedances agreed with those reported in literature for healthy patients [Navajas et al. 1988]. Chirps' input impedances presented high variability at frequencies under 3Hz. This is because low frequencies were corrupted by respiration and cardiac components. Correlation factors between both input impedances were calculated omitting these frequencies under 3Hz. Results showed agreements for all patients over r > 0.95.

Similar comparison was carried for the sinusoidal and chirp flow rates for each electrode configuration and subject (Figure 5). Likewise, respiration and cardiac components corrupted the chirps at frequencies under 3Hz. Correlation factors for frequencies under 3Hz were found over r>0.8.

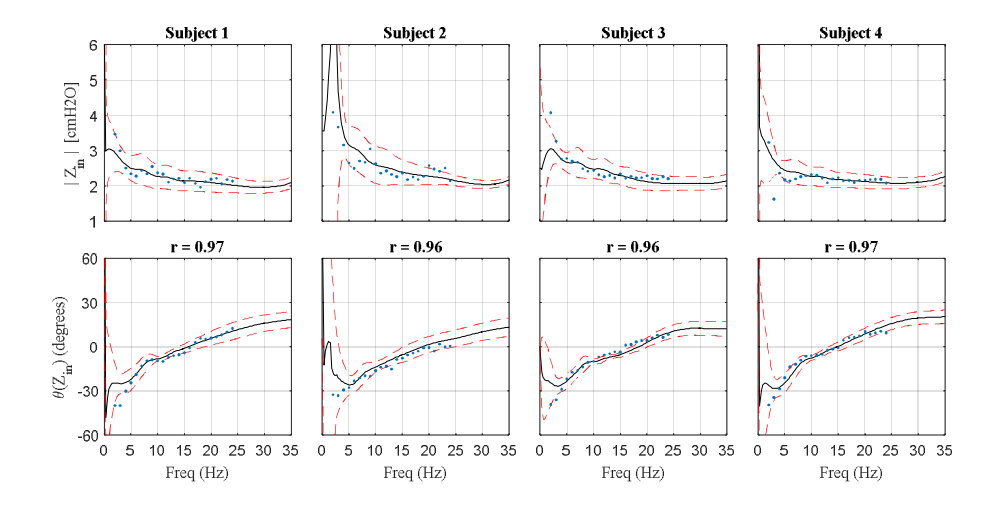


Figure 4. Input impedance for the four subjects. Upper plots present the magnitude and lower plots the phase for frequencies between 0 to 35Hz. Solid lines are the averaged input impedances computed from chirp windows, and dash line its variance. Dots are the input impedances calculated from each individual sinusoid. r is the correlation between chirp and sinusoid input impedances.

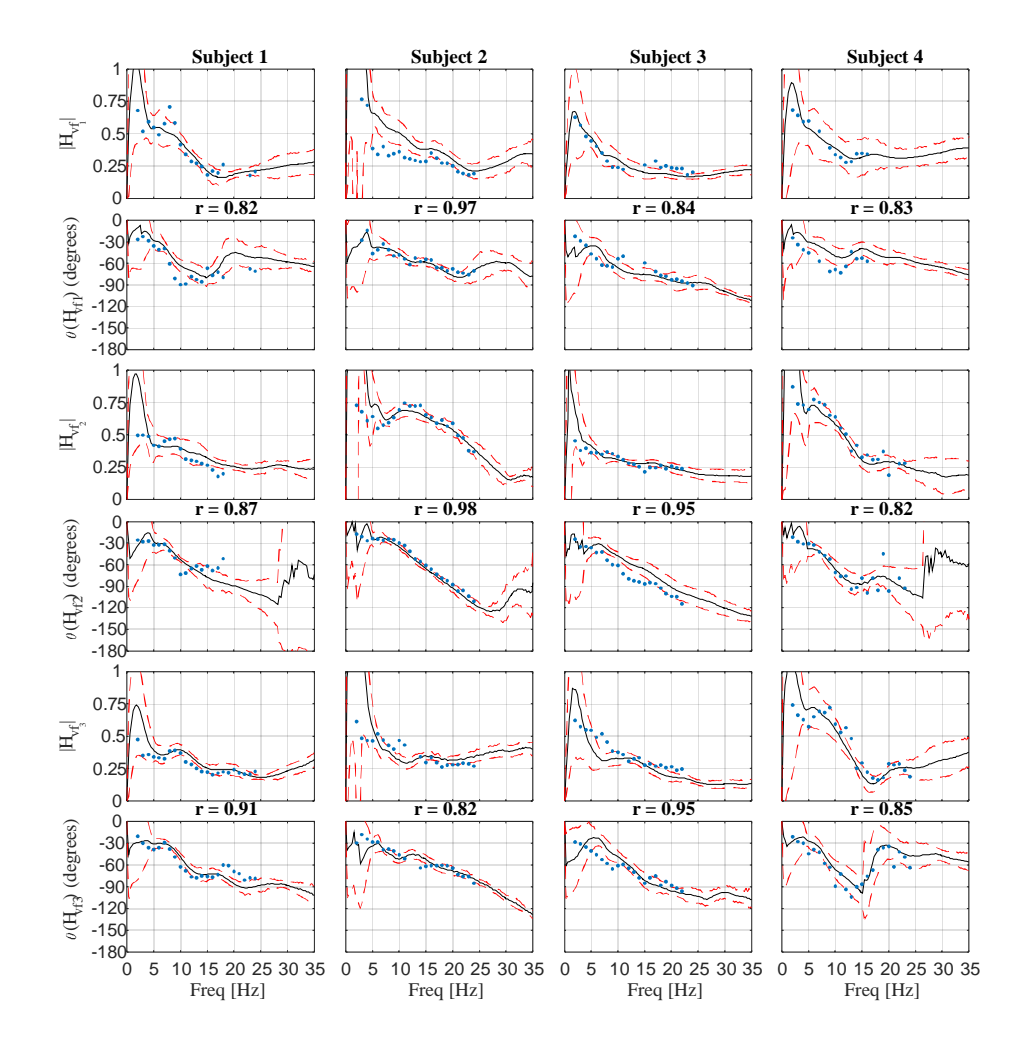


Figure 5. Flow ratios for the three electrode configurations and four subjects. Row plots are grouped by pairs magnitude-phase for the upper (m=1), middle (m=2), and lower (m=3) electrode configurations. Solid lines are the averaged flor ratios computed from chirp windows, and dash line its variance. Dots are the flow rates calculated from each individual sinusoid. r is the correlation between chirp and sinusoid flow ratios.

Flow ratio describes how an arbitrary amplitude and frequency flow oscillation at the airway opening is reflected in the equivalent to air flow in the lung tissue. Magnitude tells the amplitude of the tissue oscillations relative to airway opening oscillations. Phase tells its delay in degrees. All magnitudes for all flow ratios were smaller than one, as no all the airway opening flow may reach the tissue. All phases were negative indicating causation.

Although, flow ratios showed low consistency between electrode configurations and subjects, all presented a similar antiresonance frequency response; A point in frequency with minimum magnitude accompanied by a large shift in phase. Figure 6 plots together the different electrode configurations' flow ratios for each subject, and indicates their antiresonace frequency.

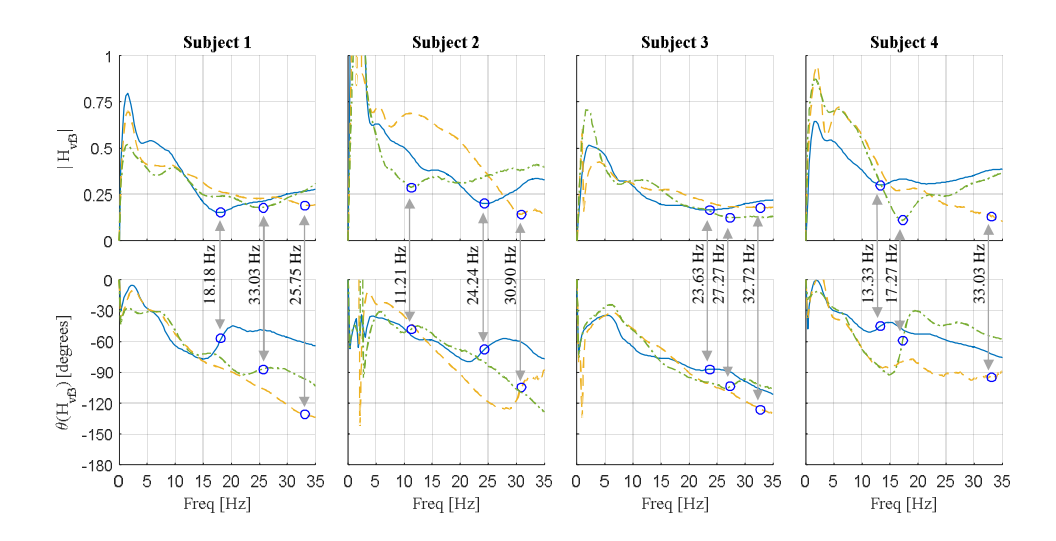


Figure 6. Comparison of flow ratios by electrode configuration within each subject. Upper plots present the magnitude and lower plots the phase for frequencies between 0 to 35Hz. Different line correspond to different electrode configuration: solid line upper (m=1); dashed line middle (m=2); and dotted line lower (m=3). Circles mark the antiresonant frequency for each flow ratio.

In order to assess flow ratio changes with lung volume, chirp windows were separated into three groups depending whether the averaged value of the IP window felt in the lower, middle, or upper third of the tidal volume. Flow ratios were averaged for each group. Figure 7 plots the results for the three electrode configurations of subject-1. For the upper electrode configurations where the antiresonance effect was more noticeable, increase of the effect with the decrease in lung volume was observed. For the middle and lower electrode configurations same behavior had smaller result.

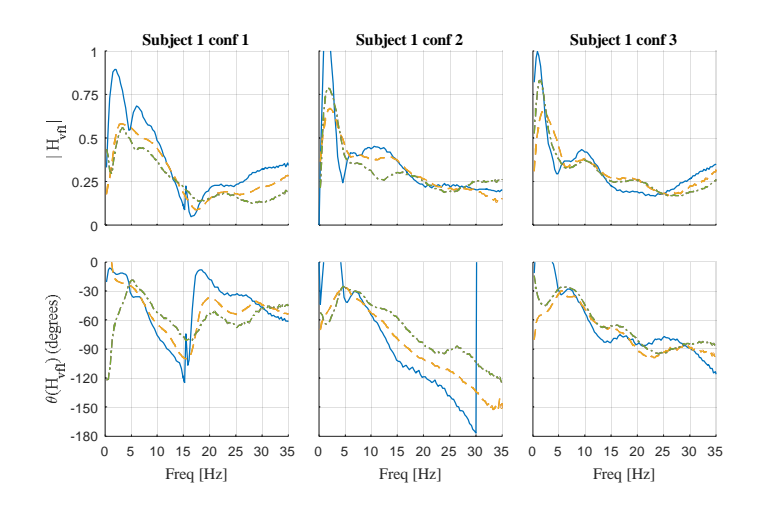


Figure 7. Comparison of the flow ratios by tidal volume level for the three electrode configuration of subject-1. Upper plots present the magnitude and lower plots the phase for frequencies between 0 to 35Hz. Different lines correspond to the average of flow ratios falling into three different tidal volume levels; solid line to upper third; dashed line to middle third; and dotted line to lower third.

4. Discussion

After comparison with traditional sinusoidal oscillations, chirp oscillations prove to be a valid FOT method for measuring both input impedance and flow ratios. Moreover, chirps enable a better resolution for high frequencies in the IP signal that other pressure oscillations waves. IP track volume changes. Therefore, for constant amplitude flow oscillations at the mouth the amplitude of IP oscillations decreases with frequency at a rate of $1/2\pi f$. For impulse oscillometry or pseudorandom noise high frequencies may become too small to be measured by IP with accuracy [Gracia et al. 2011] [Gracia et al. 2015].

We believe that flow ratios' results cannot be explained with the initial assumption that oscillations in the IP signal are solely related to volume changes in the alveoli. Based on the traditional six-element model of the respiratory system (Figure 8) [Bates, 2009], we would expect a flow ratio with a smooth decrease in magnitude and flow with increasing frequency. In our opinion, volume oscillations in the alveoli occur and regulate thoracic electrical resistivity. However, they coexist with another phenomenon translating FOT oscillations into the IP signal. The overlapping of both phenomena causes a destructive interference at the antiresonace frequency. We identify two possible causes for this phenomenon: alveolar pressure oscillations modulating pulmonary capillaries blood volume; or skin-electrode interface vibrations causing a synchronous motion artifact.

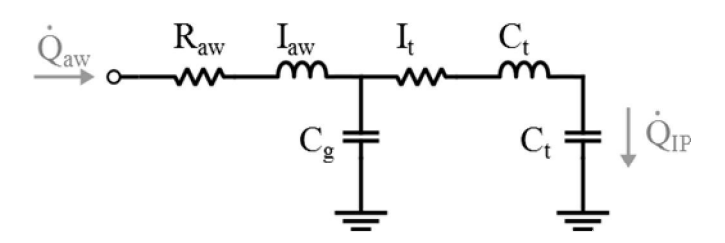


Figure 8. Six-element model of the respiratory system. Where the input of the circuit corresponds to airway opening flow \dot{Q}_{ao} , and the time derivative of the IP signal \dot{Q}_{IPm} equals the flow through the lung tissue impedance. Elements correspondence: R_{aw} airway resistance; I_{aw} airway inductance; R_t tissue resistance; I_t tissue inertance; C_t tissue compliance; C_g alveolar gas compression;

Alveolar pressure

The largest contributor to the lung tissue electrical resistance comes from the low resistivity blood filled in the pulmonary capillaries [Nopp et al. 1997]. The amount of blood volume in these capillaries is governed by pleural and alveolar pressures [Liu et al. 1998]. Therefore, pressure oscillations in the alveoli may modulate the pulmonary capillaries blood volume leading to proportional changes in tissue resistivity density. Studies using alveolar capsules show very different response to FOT oscillations for alveolar pressure and alveolar volume [Fredberg et al. 1985].

This hypothesis would explain why the antiresonant effect is more visible in the upper electrode configuration. IP signal in this configuration has a higher contribution from first and second perfusion zones. Alveolar pressure oscillations may drive the recruitment and distension of alveolar vessels in these zones. Moreover, the reduction in antiresonat effect with the increase of lung volume could be caused by the stiffening of the alveolar walls (Figure 6).

Alveolar pressure is nonhomogeneously distributed in the lungs [Fredberg et al. 1985]. Therefore, this effect may be sensitive to the electrodes location, thus explaining the lack of consistency between subjects.

Electrode vibrations

Another possibility is that FOT oscillations vibrate body tissues from the lungs to the skinelectrode interface. Vibrations at this point produce a motion artefact at the same frequency than the FOT oscillation that couples with the IP signal.

According to this hypothesis, increase lung volume may increase the stiffness of the skin in the thorax reducing vibrations, thus reducing the antiresonat effect. Moreover, results would be sensitive to the electrodes location, explaining the lack of consistency between subjects.

5. Conclusions

We conducted a preliminary study showing the combined use of FOT and thoracic electrical impedance measurement. The use of chirps as the FOT pressure excitation signals was validated in a comparison with traditional sinusoid oscillations. Flow ratios assessed in four subjects and at three thorax levels suggest that alveolar volume changes are not the only cause of oscillation in the IP signal. Either, alveolar pressure oscillations or unwanted vibration on the electrodes interact IP signal. The combined FOT-IP method needs further analysis, improvement in the accuracy of instruments, and larger clinical study samples.

Appendix A

Calculation of input impedance and it's coherence fuction

Respiratory input impedance (Z_{in}) is the transfer function between mount forced pressure and its flow response. It is a complex and frequency dependent value. Coherence function is an index of causality between the input and output of a linear system. It is a real number between 0 and 1, also relative to each frequency. The most common mode to compute these values from time series is using the cross spectrum function as suggested by Michaelson et al. [Michaelson et al. 1975]:

$$Z_{in}(\mathbf{w}) = \frac{G_{pf}(\mathbf{w})}{G_{ff}(\mathbf{w})} \tag{2}$$

$$g^{2}_{in}(w) = \frac{\left|G^{2}_{pf}(w)\right|}{G^{2}_{ff}(w) \times G^{2}_{pp}(w)}$$
(3)

where

 G_{pf} = cross spectrum between airway opening pressure (P_{ao}) and airways flow (\dot{Q}_{ao});

 G_{ff} = autocorrelation spectrum of Q_{ao} ;

 G_{pp} = autocorrelation spectrum of P_{ao} ;

Appendix B

Calculation of flow ratio and it's coherence fuction

Flow ratio (H_{vf}) is the transfer function between mount forced flow and its response in the IP signal. IP signal tracks air volume changes in the lung tissue. Therefore, it needs to be differentiated to flow for this comparison. This is achieved by dividing the transfer function of flow to IP volume by $-j\omega$. Since G_{vf} equals $-j\omega$ G_{vf} [Aliverti et al. 2001].

$$H_{\psi f}(W) = \frac{-H_{vf}}{jW} = \frac{-1}{jW} \times \frac{G_{vf}(W)}{G_{ff}(W)}$$
(4)

$$g^{2}_{vf}(w) = \frac{\left|G^{2}_{vf}(w)\right|}{G^{2}_{vv}(w) \times G^{2}_{ff}(w)} = \frac{w^{2} \times \left|G^{2}_{if}(w)\right|}{w^{2} \times G^{2}_{ifi}(w) \times G^{2}_{ff}(w)} = g^{2}_{if}(w)$$
(3)

where

 G_{vf} = cross spectrum between airway opening flow (\dot{Q}_{ao}) and IP volume (Q_{IPm})

 G_{ff} = autocorrelation spectrum of \dot{Q}_{ao} ;

 G_{vv} = autocorrelation spectrum of Q_{IPm} ;

References

Aliverti A, Dellaca R, Pedotti A. Transfer impedance of the respiratory system by forced oscillation technique and optoelectronic plethysmography. *Annals of biomedical engineering*, 29(1):71–82, 2001.

Bates J H. Lung mechanics: an inverse modeling approach. Cambridge University Press. 2009.

Bauer BB. Equivalent circuit analysis of mechano-acoustic structures. Transactions of the IRE. AU-2:112-120, 1954.

Berger KI, Goldring RM, Oppenheimer BW. Point: Should Oscillometry Be Used To Screen For Airway Disease? Yes. *Chest*, 148(5):1131-1135, 2015;

Brusasco V, Schiavi E, Basano L, and Ottonello P. Comparative evaluation of devices used for measurement of respiratory input impedance in different centres. Eur Respir Rev. 4:118 –120, 1994.

Fredberg JJ, Ingram RH, Castile RG, Glass GM, Drazen JM. Nonhomogeneity of lung response to inhaled histamine assessed with alveolar capsules. *Journal of Applied Physiology*, 58(6), 1914-1922, 1985.

Gracia J, Seppä V, Viik J. Combining Impulse Oscillometry and Multi-Lead Impedance Pneumography for Regional Analysis of Dynamic Lung Function. *European Respiratory Journal*.(42) Suppl 57, 2014.

Gracia J, Seppä V, Viik J. Multilead impedance pneumography and forced oscillation technique for assessing lung tissue mechanical properties. In proceedins of the The 10th International Conference on Bioelectromagnetism, 2015.

Hantos Z, Daroczy B, Suki B, Nagy S, Fredberg JJ. Input impedance and peripheral inhomogeneity of dog lungs. *Journal of Applied Physiology*, 72(1):168-178, 1992.

Liu, C. H., et al. Airway mechanics, gas exchange, and blood flow in a nonlinear model of the normal human lung. *Journal of applied physiology* 84 (4):1447-1469, 1998.

Michaelson ED, Grassman ED, Peters WR. Pulmonary mechanics by spectral analysis of forced random noise. *Journal of Clinical Investigation*. 56(5): 1210-1216, 1975.

Navajas D, Farre R, Rotger MM, Milic-Emili J, Sanchis J. Effect of body posture on respiratory impedance. *Journal of Applied Physiology*, 64(1):194–199, 1988.

Nopp P, Harris N, Zhao TX, Brown B. Model for the dielectric properties of human lung tissue against frequency and air content. *Medical and Biological Engineering and Computing*, 35(6): 695–702, 1997.

Peslin R, Fredberg JJ. Oscillation mechanics of the respiratory system. Comprehensive Physiology, 12:145-177, 2011.

Seppä V, Hyttinen J, Viik J. A method for suppressing cardiogenic oscillations in impedance pneumography. *Physiological measurement*. 32(3),337, 2011.